Article

Hydrological and Meteorological Controls on Large Wildfire Ignition and Burned Area in Northern California during 2017–2020

Yusuke Hiraga * and **M. Levent Kavvas**

Hydrologic Research Laboratory, Department of Civil and Environmental Engineering, University of California, Davis, CA 95616, USA; mlkavvas@ucdavis.edu

* Correspondence: yhiraga@ucdavis.edu

Abstract: This study examined the hydrological/meteorological controls on large wildfires > 10,000 acres (40.5 km^2) during 2017–2020 in Northern California at spatial and temporal scales of the target wildfires' occurrence or growth. This study used the following simple indices for analysis: Moisture Deficit Index (MDI) computed by dividing vapor pressure deficit by soil moisture, MDIWIND computed by multiplying MDI by horizontal wind speed, and MDIGUST computed by multiplying MDI by wind gust speed. The ignition location MDIWIND and MDIGUST showed larger values on the ignition date in fire-years compared to non-fire-years for most of the target wildfires (95.8% and 91.7%, respectively). The peak timing of MDIGUST, which is to evaluate the integrated effect of dry atmosphere/soil and windy condition, coincided with the ignition date for August Complex Fire 2020, Ranch Fire 2018, Claremont-Bear Fire 2020, and Camp Fire 2018. We also found that August Complex Fire 2020, Claremont-Bear Fire 2020, and Camp Fire 2018 occurred in the areas where MDIGUST became spatially and temporally high. Further, strong relationships were found between burned area sizes of the target wildfires and MDI (R = 0.62, *p* = 0.002), MDIWIND (R = 0.72, *p* < 0.001), and MDIGUST (R = 0.68, *p* < 0.001). Overall, the findings in this study implied the strong effect of dry atmosphere/soil and windy conditions on recent large wildfire activities in Northern California. The findings could contribute to a more temporally and spatially detailed forecast of wildfire risks or a better understanding of wildfires' occurrence and growth mechanisms.

Keywords: wildfire; climate change; atmospheric moisture; soil moisture; forest; drought; wind gusts; fire weather; forecast

1. Introduction

California has experienced numerous wildfires and their associated damages in recent years. During 2017–2020, over 34,000 wildfires burned about 8 million acres (32,375 km^2), accounting for more than 7% of California's land area [1]. The California Department of Forestry and Fire Protection (CALFIRE) reported that these recent wildfires including both California's largest wildfire in history: August Complex Fire 2020 and its deadliest wildfire in history: Camp Fire 2018, which caused over 180 fatalities and damaged or destroyed over 45,000 structures [1]. Recent extreme wildfires have substantial economic, social, and environmental impacts. Wang et al. [2] estimated total wildfire damages in 2018 to be USD 148.5 billion, with USD 27.7 billion (19%) in capital losses, USD 32.2 billion (22%) in health costs due to air pollution exposure, and USD 88.6 billion (59%) in indirect losses related to broader economic disruption. Proctor et al. [3] stated that drinking water quality exceeded state and federal government-defined exposure limits for volatile organic compound contaminants in Tubbs Fire 2017 and Camp Fire 2018 in Northern California.

It is well established that recent wildfire activity has been strongly driven by hydrological/meteorological conditions [4–16]. The recent increase in California wildfire activity has been driven by hotter temperature-induced moisture deficit increase [4,5],

decrease in fire-season precipitation frequency [6], and earlier snowmelt-induced snow-pack decrease [7,8]. Strong winds and gusts also play a critical role in both initiating and supporting the fires, such as "Diablo" for Northern California or "Santa-Ana" for Southern California [9–13]. On the basis of the fact that wildfire activity has been strongly driven by hydrological/meteorological conditions, future wildfire activity is expected to be worse with climate change in California, such as significant increases in large wildfire occurrence and burned area [17,18]. Therefore, it is becoming more important to further understand the hydrological/meteorological controls on wildfire activity in California. In particular, investigating the hydrological/meteorological controls on wildfire regimes at finer scales, such as spatial and time scales of individual wildfire's ignition or growth, is essential for a better understanding of wildfires' occurrence and growth mechanisms. This investigation is also expected to result in a more temporally and spatially detailed wildfire occurrence and growth forecast.

There have been several studies characterizing hydrological/meteorological conditions conducive to historical large wildfire activities at spatial and time scales of individual wildfire's ignition or growth in California. For instance, Nausler et al. [10] showed that wildfires in the California North Bay region in October 2017 occurred coincident with strong downslope winds, with a majority of burned area occurring within the first 12 h of ignition. Di Giuseppe et al. [19] showed that observed California fires in 2017 were matched to high values of Canadian Fire Weather Index (FWI) influenced by temperature, relative humidity, precipitation, and wind speed [20]. Westerling et al. [21] found that the National Fire Danger Rating System (NFDRS) Burning Index (BI), which mainly is determined from the moisture content of a forest and wind speed, showed the increase during the period that Ceder Fire 2003 started and grew due to Santa Ana wind. More recently, Srock et al. [22] showed the linkage between the developed Hot–Dry–Windy index (HDW), which evaluates the comprehensive effect of atmospheric moisture, temperature, and wind speed, as well as the day on which the most rapid fire growth occurred for some historical large wildfires including Ceder Fire 2003 in Southern California at specified points.

As listed above, the previous studies investigated the hydrological/meteorological controls on historical large wildfire activities in California, mainly focusing on atmospheric moisture, temperature, and wind speed [22–24]. What seems to be lacking, however, is an investigation on hydrological/meteorological controls on more recent California wildfires, such as in 2020, the most significant wildfire season recorded in California's modern history [1], at spatial and time scales of individual wildfire's ignition or growth. Thus, this study was designed to evaluate the hydrological/meteorological controls on more recent large wildfires during 2017–2020 in California at spatial and temporal scales of the wildfires' occurrence or growth. Furthermore, this study considered the soil moisture to examine the hydrological/meteorological controls in addition to atmospheric moisture, temperature, and wind speed considered in the previous studies. This is because several recent studies have reported that soil moisture plays very important role in controlling wildfire activity [25–34]. For instance, Thomas Ambadan et al. [28] stated that soil moisture is potentially useful in identifying soil moisture anomalies where wildfire hot-spots may occur. Rigden et al. [31] concluded that using soil moisture, as opposed to vapor pressure deficit (VPD) alone, has the important implication of greater predictability of wildfire risk. Here, VPD is the difference between the water vapor pressure at saturation and the actual water vapor pressure for a given temperature. Moreover, this study addresses not only examining the hydrological/meteorological characteristics on the day with wildfire activity at a specified point, which has been mainly done by previous studies [21,22], but also addresses investigating the spatial distribution of hydrological/meteorological indices to identify wildfire hot-spots, as well as investigating the relationships between hydrological/meteorological indices and wildfire area burned at the scale of wildfire growth to understand the hydrological/meteorological controls on wildfire growth.

This study analyzed 24 large wildfires whose burned areas were larger than 10,000 acres (40.5 km^2) and that were located in North Coast and Sierra Nevada in Northern California.

Northern California was selected as a study area since recent unprecedented wildfire activities have predominantly been in Northern California. The structure of this paper is as follows: Section 2 of this paper reviews the study area, hydrological and meteorological data, and analysis methods. Section 3 presents the results of the analysis. Section 4 discusses these results and summarizes the findings.

2. Materials and Methods

2.1. Study Area and Target Wildfire

This study examined the recent large wildfires, located in the regions of North Coast and Sierra Nevada within the study area over Northern California (Figure 1).
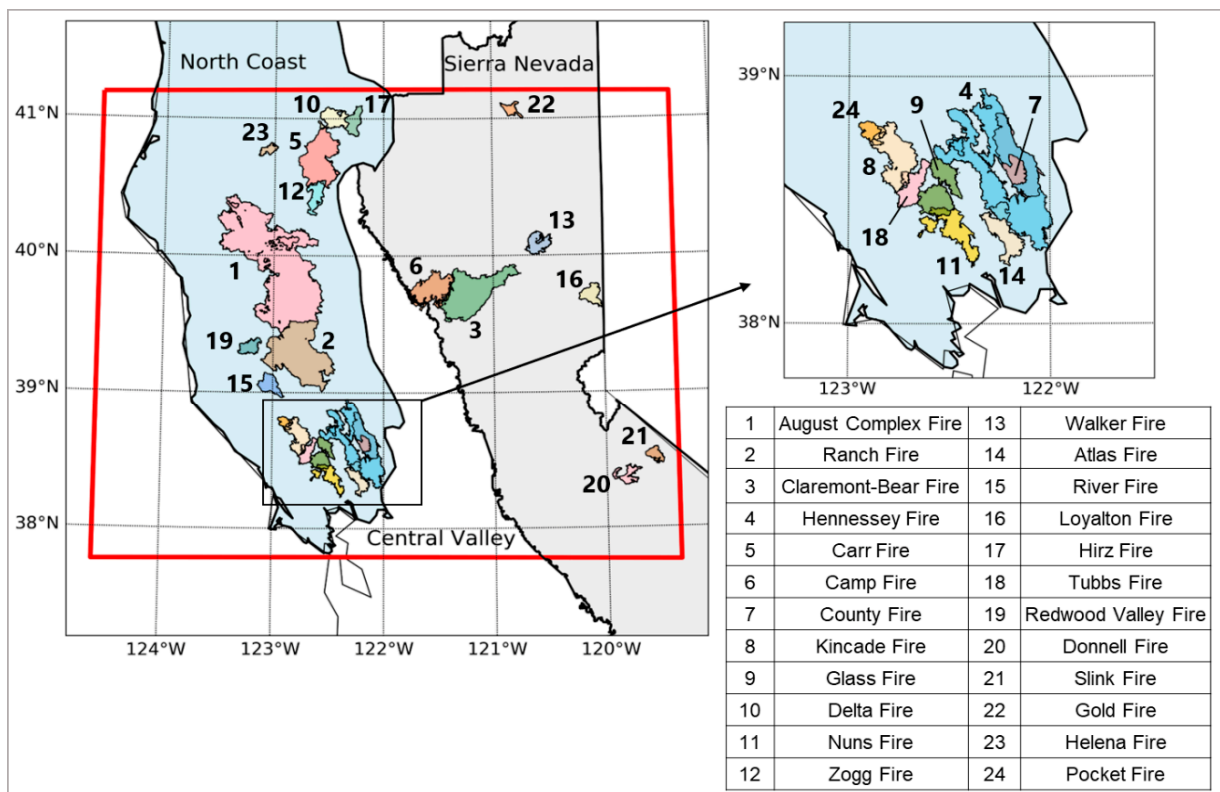

1	August Complex Fire	13	Walker Fire
2	Ranch Fire	14	Atlas Fire
3	Claremont-Bear Fire	15	River Fire
4	Hennessey Fire	16	Loyalton Fire
5	Carr Fire	17	Hirz Fire
6	Camp Fire	18	Tubbs Fire
7	County Fire	19	Redwood Valley Fire
8	Kincade Fire	20	Donnell Fire
9	Glass Fire	21	Slink Fire
10	Delta Fire	22	Gold Fire
11	Nuns Fire	23	Helena Fire
12	Zogg Fire	24	Pocket Fire

Figure 1. Study area and target wildfires. The study area is shown in a red frame. North Coast and Sierra Nevada are shown in light blue and light green, respectively. The Central Valley separates the North Coast and Sierra Nevada regions.

North Coast and Sierra Nevada are defined as shown in Figure 1. Over these two largely forested regions, lightning accounts for the majority of summer wildfire ignitions [35]. Our study targeted 24 large wildfires whose burned areas were larger than 10,000 acres (40.5 km^2), occurring during 2017–2020. In this paper, these wildfires are called "target wildfires". The wildfires that were not fully extinguished by November 2020 were not targeted. We also excluded the wildfires whose burned areas did not contain the atmospheric and surface grid point data. Table 1 lists the target wildfires' burned areas, ignition date, extinguished date, and ignition location latitude and longitude information, which came from the CALFIRE Incident Archive dataset [1] and Incident information system dataset [36].

Table 1. Target wildfire information.

Target Wildfires	Burned Area (Acres)	Ignition Date	Extinguished Date	Ignition Latitude	Ignition Longitude
August Complex Fire	1,032,648	16 August 2020	11 November 2020	39.776	−122.673
Ranch Fire	410,203	27 July 2018	4 January 2019	39.243	−123.103
Claremont−Bear Fire	318,935	17 August 2020	30 November 2020	39.691	−121.227
Hennessey Fire	317,909	17 August 2020	2 October 2020	38.482	−122.149
Carr Fire	229,651	23 July 2018	30 August 2018	40.654	−122.624
Camp Fire	153,336	8 November 2018	25 November 2018	39.813	−121.435
County Fire	90,288	30 June 2018	4 January 2019	38.806	−122.182
Kincade Fire	77,758	23 October 2019	6 November 2019	38.792	−122.780
Glass Fire	67,484	27 September 2020	20 October 2020	38.563	−122.497
Delta Fire	63,311	5 September 2018	4 January 2019	40.943	−122.430
Nuns Fire	56,556	8 October 2017	9 February 2018	38.349	−122.503
Zogg Fire	56,338	27 September 2020	13 October 2020	40.539	−122.567
Walker Fire	54,612	4 September 2019	26 September 2019	40.061	−120.681
Atlas Fire	51,624	8 October 2017	9 February 2018	38.392	−122.244
River Fire	48,920	27 July 2018	4 January 2019	39.048	−123.120
Loyalton Fire	47,029	14 August 2020	14 September 2020	39.702	−120.143
Hirz Fire	46,150	9 August 2018	4 January 2019	40.896	−122.219
Tubbs Fire	36,807	8 October 2017	9 February 2018	38.609	−122.629
Redwood Valley Fire	36,523	8 October 2017	9 February 2018	39.249	−123.166
Donnell Fire	36,450	1 August 2018	4 January 2019	38.349	−119.929
Slink Fire	26,759	29 August 2020	9 October 2020	38.568	−119.568
Gold Fire	22,634	20 July 2020	12 August 2020	41.110	−120.923
Helena Fire	18,709	31 August 2017	9 January 2018	40.760	−123.100
Pocket Fire	17,357	9 October 2017	9 February 2018	38.765	−122.909

Figure 1 shows the locations and perimeters of the target wildfires. The perimeters of the wildfires during 2017 and 2018 were obtained from the Monitoring Trends in Burn Severity Project (MTBS) dataset [37]. MTBS delineates fire perimeters using pre- and post-fire satellite imagery along with Normalized Burn Ratio (NBR), differenced NBR, and relativized differenced NBR images [37]. The wildfire perimeters during 2019 and 2020 came from the California State Geoportal Wildfire perimeters dataset [38]. As shown in Figure 1 and Table 1, the target wildfires included August Complex Fire 2020 and Ranch Fire 2018, which are the largest and second-largest wildfires in California's modern history, respectively. The target wildfires also included Camp Fire 2018, which is the deadliest wildfire in California's modern history.

2.2. Hydrological and Meteorological Data

This study used data for hydrological/meteorological gridded variables, obtained from the National Centers for Environmental Prediction (NCEP) North American Mesoscale (NAM) 12 km Analysis [39]. NCEP NAM 12 km Analysis provides the mesoscale atmospheric and surface analysis grids over the continental United States at 12 km spatial resolution every 6 h for 2012 to the present. NCEP NAM 12 km Analysis was produced by the Weather Research and Forecasting Non-Hydrostatic Mesoscale Model (WRF-NMM). This study investigated the hydrological/meteorological controls on the target wildfires using the following variables: VPD at 2 m above ground, horizontal wind speed at 10 m above ground, wind gust speed at surface level, and average soil moisture content from

land surface to 2 m depth below ground. VPD is calculated using the temperature and relative humidity at 2 m above ground, as shown in Equation (1).

$$\text{VPD} = e_s - e \tag{1}$$

where e_s and e are saturated vapor pressure and actual vapor pressure (hPa), respectively. e_s is computed using the following equation [40]:

$$e_s = 6.112 \times exp\left(\frac{17.67 T_a}{T_a + 243.5}\right) \tag{2}$$

where T_a is the land air temperature at 2 m above ground (°C).

Namely, VPD describes the aridity of the atmosphere. Wind gust speed represents the maximum wind speed observed over a fixed period [41]. We selected the aforementioned state variables since it is well established that hot, dry, windy weather and dry surface/forest play important roles for wildfire activities [22,42,43]. This study used the variables at or close to the surface for the analysis since they are considered to affect more directly the ignitions and growths of wildfires compared to the variables at higher heights. Average soil moisture content from land surface to 2 m depth below ground was used since water available to plants is generally considered to be in the upper 2 m of soil [44]. NCEP NAM 12 km Analysis computes wind gust speed by adding the fraction of the wind speed difference between the top of the planetary boundary layer (PBL) and the surface, which is mixed down to the surface to the surface wind speed [45]. In this process, PBL height is determined on the basis of a critical value of the bulk Richardson number [45].

Besides the variables above, we used the following simple indices that are meant to evaluate the hydrological/meteorological controls on the wildfires more comprehensively.

- Moisture Deficit Index (MDI), which is computed by dividing VPD by soil moisture content;
- MDIWIND, which is computed by multiplying MDI by horizontal wind speed;
- MDIGUST, which is computed by multiplying MDI by wind gust speed.

MDI is used to describe the comprehensive aridity of both atmosphere and soil. MDI can also be considered to address drought stress on vegetation by capturing the strength in water potential differences between the atmosphere and soil, with vegetation and prominent pass-through or link between the two. MDIWIND and MDIGUST are to evaluate the integrated effect of hot, dry, and windy conditions on the ignition and burned area of the target wildfires.

2.3. Analysis

First, we analyzed the characteristics of the hydrological/meteorological variables at the ignition location on the ignition date for each target wildfire. As the ignition location variables for each target wildfire, the aforementioned variables at the grid point that is closest to the ignition location and is located within the burned area of the wildfire were identified and used. Then, the ignition location variables on the ignition date in the year with the target wildfire were compared to the corresponding variables at the same location on the same date in years without wildfires. In this study, the variables in years without wildfires are called "non-fire-year variables". For each target wildfire, non-fire-year averaged ignition location variables were obtained by time-averaging the variables at the ignition location and on the same date as the ignition date during years up to the year before the wildfire occurred. For instance, for a target wildfire in 2019, the ignition location variables on the ignition date in 2019 were compared to the corresponding non-fire-year averaged ignition location variables during 2012–2018. The time period used to compute the non-fire-year averaged variables was from 2012 since the temporal range of the NAM 12 km Analysis is from 2012 to the present. The non-fire-year averaged values were calculated on the basis of the values in years up to the year before the occurrence of the wildfire since the land cover is often significantly different for the pre-fire and post-fire

conditions. We also conducted Welch's *t*-test in order to check if there is a statistically significant difference in the averaged ignition location variables/indices between relatively large (>50,000 acres) wildfire group and relatively small (<50,000 acres) wildfire group. R version 4.0.5 was used for performing Welch's *t*-test. In this study, a *p*-value less than 0.05 was considered statistically significant.

Second, we investigated how the temporal changes in the ignition location indices corresponded to the ignitions or growths of the selected wildfires. The time series of the daily ignition location indices, MDI, MDIWIND, and MDIGUST, during the time period from three weeks before the ignition date to one week after the ignition date were examined for each selected wildfire. The motivation of this analysis was to find key indices that can explain the timing of wildfire ignitions or growths, leading to improving the wildfire danger predictability.

Third, we examined how the spatial distribution of hydrological/meteorological indices is linked to the spatial distribution of extremely large wildfires over the study area. We investigated the relationship between the spatial distribution of daily averaged MDI-GUST and the locations of the selected wildfires on the ignition date over the study area. The motivation of this analysis is that a more detailed identification of the high wildfire risk locations may be possible by considering the spatial distribution of the hydrological/meteorological conditions.

Finally, we analyzed the relationships between the burned areas and the hydrological/meteorological variables and indices at a longer time scale and larger spatial scale for the target wildfires. In this analysis, for each target wildfire, we identified the daily spatial maximum value of the target variables/indices within the burned area and averaged the daily spatial maximum values over a 2 week period after the ignition date. For soil moisture content, we identified the daily spatial minimum value within the burned area and averaged it over a 2 week period after the ignition date. Then, the relationship between these time-averaged variables/indices and the logarithm of burned areas for target wildfires was examined. This analysis was based on the assumption that the burned area maximum/minimum variables/indices over a period of wildfire growth may explain burned areas (i.e., wildfire sizes) better than the ignition location variables/indices on the ignition date. Since the shortest fire duration was 2 weeks out of all the durations of the target wildfires in this study (Kincade fire 2019; Table 1), we performed a 2 week averaging to the variables/indices as the wildfire growth period. We used the logarithms of burned areas since it has been reported that burned area shows an exponential distribution [4,43,44].

3. Results

3.1. Characteristics of Hydrological/Meteorological Variables and Indices at the Ignition Location on the Ignition Date for the Target Wildfires

We first analyzed the characteristics of the hydrological/meteorological variables at the ignition location on the ignition date for each target wildfire by comparing them with the corresponding non-fire-year averaged ignition location variables. Table 2 shows the values of hydrological/meteorological variables at the ignition location on the ignition date for each target wildfire.

Table 2. Daily averaged hydrological/meteorological variables at the ignition location on the ignition date for each target wildfire. Each variable's ratio represents the ratio of the daily averaged ignition location variables in the fire-year to the corresponding non-fire-year averaged variables.

Target Wildfires	Burned Area (Acres)	Vapor Pressure Deficit [hPa]	Ratio (%)	Soil Moisture (%)	Ratio (%)	Horizontal Wind Speed (m s^{-1})	Ratio (%)	Wind Gust Speed (m s^{-1})	Ratio (%)
August Complex Fire	1,032,648	28.76	123.45	0.115	67.16	2.35	141.91	3.60	218.90
Ranch Fire	410,203	25.21	112.96	0.137	78.58	2.37	120.32	3.24	161.84
Claremont-Bear Fire	318,935	27.34	128.25	0.128	89.76	2.75	114.54	3.67	162.41
Hennessey Fire	317,909	31.17	214.30	0.122	99.15	1.62	64.70	1.67	66.23
Carr Fire	229,651	26.22	114.09	0.128	80.25	1.80	77.49	1.55	50.18
Camp Fire	153,336	11.42	252.97	0.121	64.04	5.12	172.54	8.16	152.36
County Fire	90,288	30.45	126.62	0.188	92.02	2.44	127.86	2.76	120.72
Kincade Fire	77,758	27.99	362.90	0.120	84.99	3.76	255.03	6.89	364.10
Glass Fire	67,484	20.36	158.83	0.126	81.09	2.79	163.06	4.44	215.93
Delta Fire	63,311	22.47	130.53	0.082	69.55	2.07	87.37	2.80	86.05
Nuns Fire	56,556	21.79	179.27	0.207	104.24	5.34	265.42	9.62	433.16
Zogg Fire	56,338	18.72	97.58	0.126	87.14	3.61	192.35	7.66	277.40
Walker Fire	54,612	14.25	98.88	0.060	69.18	1.07	52.32	2.98	83.76
Atlas Fire	51,624	21.00	153.37	0.091	99.89	6.56	311.03	11.70	484.32
River Fire	48,920	22.27	103.62	0.130	76.56	2.22	120.12	3.22	145.82
Loyalton Fire	47,029	16.36	97.71	0.139	83.60	3.04	131.65	3.42	121.98
Hirz Fire	46,150	32.66	138.43	0.116	74.06	1.54	90.28	2.04	89.34
Tubbs Fire	36,807	21.61	164.91	0.150	102.03	4.87	261.89	9.57	456.60
Redwood Valley Fire	36,523	18.69	157.03	0.142	102.73	3.20	165.77	4.70	189.12
Donnell Fire	36,450	15.73	115.93	0.192	89.38	2.55	107.80	2.66	96.35
Slink Fire	26,759	13.88	100.15	0.197	101.51	2.76	97.79	2.49	53.16
Gold Fire	22,634	24.28	147.03	0.160	99.82	2.49	97.92	2.96	79.28
Helena Fire	18,709	29.55	191.36	0.126	107.71	1.72	99.48	1.75	70.85
Pocket Fire	17,357	15.36	127.74	0.138	99.03	1.38	82.84	1.73	83.47

As shown in Table 2, for 21 wildfires (87.5%), the fire-year VPD was greater than the non-fire-year averaged VPD. Although the fire-year VPD was shown to be smaller than the non-fire-year averaged VPD for three fires (Zogg Fire 2020, Walker Fire 2019, and Loyalton Fire 2020), the differences were less than 3%. Table 2 also shows that, for 19 wildfires (79.2%), the fire-year soil moisture was smaller than the non-fire-year averaged soil moisture. On the other hand, as shown in Table 2, the comparisons of the wind speed and wind gust speed between the fire-year and non-fire-year did not show very consistent results. Fire-year values were larger than non-fire-year averaged values for 15 wildfires (62.5%) in the wind speed and for 14 wildfires (58.3%) in the wind gust speed.

In order to evaluate the hydrological/meteorological controls on the wildfire burned areas more comprehensively, we also analyzed the characteristics of the proposed indices (MDI, MDIWIND, and MDIGUST) at the ignition location on the ignition date for each fire. Table 3 shows the comparison results between the fire-year indices and non-fire-year averaged indices for the target wildfires.

Table 3. Daily averaged hydrological/meteorological indices at the ignition location on the ignition date for each target wildfire. Each index's ratio represents the ratio of the daily averaged ignition location index in the fire-year to the corresponding non-fire-year averaged index.

Target Wildfires	Burned Area (Acres)	MDI (hPa)	Ratio (%)	MDIWIND (hPa m s^{-1})	Ratio (%)	MDIGUST (hPa m s^{-1})	Ratio (%)
August Complex Fire	1,032,648	251.12	181.75	689.41	258.95	1163.61	449.75
Ranch Fire	410,203	184.43	142.60	449.78	161.64	627.40	226.94
Claremont-Bear Fire	318,935	213.80	141.52	584.40	162.45	883.62	250.60
Hennessey Fire	317,909	254.67	212.94	363.33	108.10	413.25	114.27
Carr Fire	229,651	205.12	143.08	398.40	118.64	342.16	74.75
Camp Fire	153,336	94.19	378.28	468.40	839.02	772.60	1021.12
County Fire	90,288	161.62	133.22	448.32	189.40	505.13	177.86
Kincade Fire	77,758	234.25	402.39	893.63	991.89	1665.33	1667.50
Glass Fire	67,484	161.90	192.95	527.13	322.17	910.47	464.44
Delta Fire	63,311	274.03	186.33	630.44	186.15	901.47	191.67
Nuns Fire	56,556	105.47	173.97	563.86	372.21	986.66	600.56
Zogg Fire	56,338	148.61	104.98	505.38	190.91	1113.06	334.52
Walker Fire	54,612	236.66	130.07	301.53	72.79	898.50	131.15
Atlas Fire	51,624	230.13	154.21	1520.95	419.85	2593.35	645.94
River Fire	48,920	171.85	134.49	431.45	160.31	592.11	217.68
Loyalton Fire	47,029	117.70	113.74	447.49	154.31	529.74	144.75
Hirz Fire	46,150	280.96	185.98	469.02	182.74	585.65	172.26
Tubbs Fire	36,807	143.71	163.51	690.65	350.05	1294.55	597.46
Redwood Valley Fire	36,523	131.60	153.87	430.17	253.28	622.89	308.12
Donnell Fire	36,450	81.94	128.24	243.79	135.24	256.76	122.56
Slink Fire	26,759	70.62	98.04	201.82	104.37	196.66	53.50
Gold Fire	22,634	151.42	147.51	458.43	151.44	502.67	120.39
Helena Fire	18,709	234.68	174.20	413.19	146.12	483.70	125.54
Pocket Fire	17,357	111.48	130.10	195.27	115.54	231.50	114.92

As shown in Table 3, the fire-year ignition point MDI was larger than the non-fire-year averaged ignition point MDI for all the target wildfires except for Slink Fire 2020. This result implies that the ignition location grids for the target wildfires generally had moisture deficit tendencies on the land and in the atmosphere during the fire-years compared to non-fire-years. Table 3 also shows that the fire-year values were larger than non-fire-year averaged values for 23 wildfires (95.8%) in MDIWIND and for 22 wildfires (91.7%) in MDIGUST, which were developed to comprehensively evaluate the effects of moisture deficit and wind strength. Moreover, MDIWIND and MDIGUST showed significant differences between very large fires (>50,000 acres) and relatively small fires (<50,000 acres) in the target wildfires. Table 4 summarizes the average values and their standard deviations of the aforementioned ignition location indices for wildfires whose burned areas were larger than 50,000 acres and smaller than 50,000 acres.

Table 4. Average values and their standard deviations of the daily averaged ignition location indices.

	MDI (hPa)	MDIWIND (hPa m s^{-1})	MDIGUST (hPa m s^{-1})
1. Average value for wildfires > 50,000 acres (standard deviation)	196.86 (55.83)	596.07 (304.8)	984.04 (573.22)
2. Average value for wildfires < 50,000 acres (standard deviation)	149.60 (65.52)	398.13 (150.0)	529.62 (312.32)
Ratio of increase from 2 to 1 (%)	31.6	49.7	85.8
p-value in the difference between 1 and 2	$p = 0.082$	$p = 0.048$	$p = 0.021$

As shown in Table 4, the average ignition location MDIWIND and MDIGUST for wildfires > 50,000 acres showed 49.7% and 85.8% larger values ($p < 0.05$) than the average ignition location indices for wildfires < 50,000 acres, respectively. We can see that using the wind gust speed information lets us see a greater difference in the index values between very large fires and relatively small fires. It should be noted that the significant differences between very large fires and relatively small fires were not found in MDI and in the variables listed in Table 2. Furthermore, any statistically significant correlation between the ignition location variables/indices listed in Tables 2 and 3 and burned areas was not found. We further investigate the correlation between these variables/indices and burned areas at a longer time scale and larger spatial scale in Section 3.4.

3.2. Time Series of Ignition Location Hydrological/Meteorological Indices for the Target Wildfires

As shown in Section 3.1, the ignition location indices (MDI, MDIWIND, and MDI-GUST) showed marked differences between the fire-year and non-fire-years for the target wildfires. Therefore, we examined the time series of these indices during the period around the ignition date in order to discuss their ability to identify when the large wildfire occurrence is likely. Figure 2 shows the time series of the daily averaged ignition location indices for the three largest wildfires in this study: (a) August Complex Fire 2020, (b) Ranch Fire 2018, and (c) Claremont-Bear Fire 2020, as well as (d) the deadliest wildfire in California's history, Camp Fire 2018.
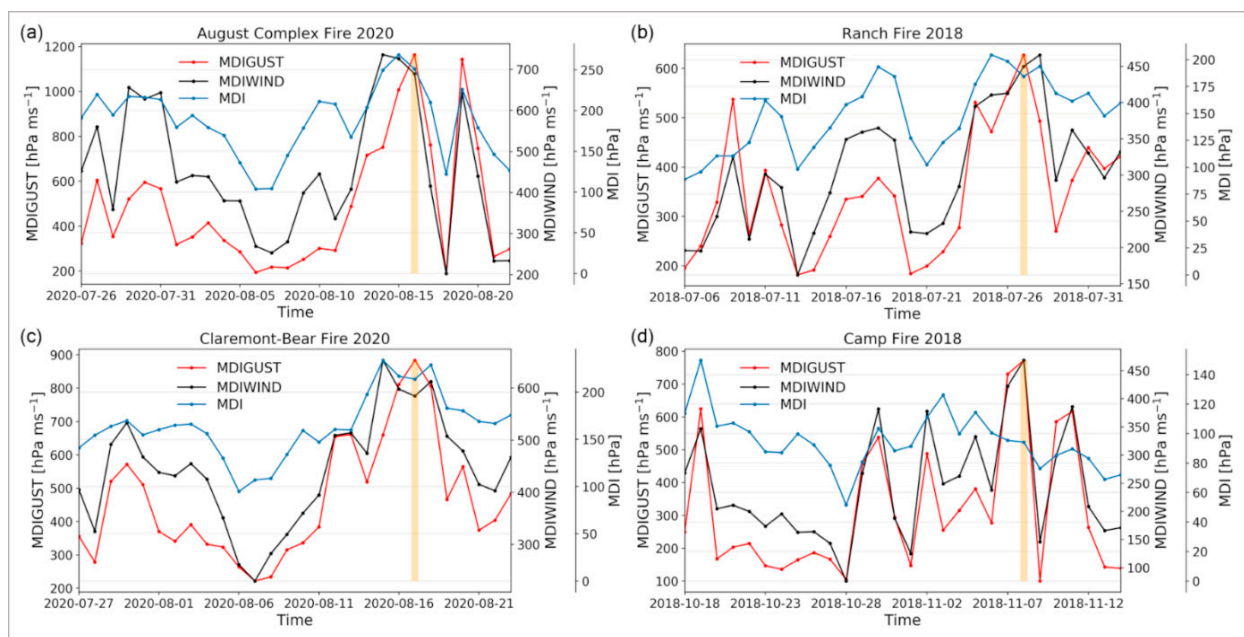

Figure 2. Time series of the daily averaged ignition location indices for each wildfire. (**a**) August Complex Fire 2020, (**b**) Ranch Fire 2018, (**c**) Claremont-Bear Fire 2020, and (**d**) Camp Fire 2018. The ignition date for each wildfire is shown as a thick orange line.

These disastrous four wildfires are targeted for the analysis in Sections 3.2 and 3.3. In Figure 2, the ignition date for each wildfire is shown by the thick orange line. As shown in Figure 2, for the above-mentioned four wildfires, MDIGUST showed its greatest value on the ignition date during the specified 4 week period (from three weeks before the ignition date to one week after the ignition date). For August Complex Fire 2020 (Figure 2a), MDIGUST gradually increased towards the ignition date from about 10 days before the ignition date, showing a more rapid increase around the ignition date.

Figure 2 shows that, for these selected wildfires, MDIWIND also became higher around the ignition date. Although MDIWIND essentially showed a trend similar to the MDIGUST trend, it peaked on the ignition date for only Camp Fire 2018 during the specified period, as shown in Figure 2d. For August Complex Fire 2020 and Claremont-Bear Fire 2020, MDIWIND peaked two days before the ignition date, showing a decreasing trend towards the ignition date.

Meanwhile, MDI did not show its greatest value on the ignition date for all the four target wildfires, although it became relatively large around the ignition date for the three largest wildfires in this study (Figure 2a–c). Furthermore, when MDI showed its large value, MDIWIND and MDIGUST were not necessarily high since wind was considered not to be very strong on those days (e.g., 18 July 2018, in Figure 2b; 3 November 2018, in Figure 2d). At the ignition location of Camp Fire 2018 (Figure 2d), we can see that MDI did not correlate strongly with MDIGUST or MDIWIND.

On the basis of the above results, we were able to find the date and time when the risk of large wildfire occurrence was high at a certain location by using the indices that comprehensively evaluate the effects of both moisture deficit and wind strength. Specifically, MDIGUST peaked on the ignition date and showed a more rapid increase around the ignition date compared to MDIWIND during the periods shown in Figure 2. These findings suggest that MDIGUST may identify the date with a high risk of disastrous wildfires at a certain location.

3.3. Spatial Distributions of Hydrological/Meteorological Index and Locations of the Target Wildfires

In this section, we analyzed the spatial distribution of MDIGUST and locations of the selected wildfires in order to assess whether we can identify the areas with a high risk of disastrous wildfire occurrences on a specified date. Figure 3 shows the spatial distributions of daily averaged MDIGUST over the study area on the ignition date of (a) August Complex Fire 2020, (b) Ranch Fire 2018, (c) Claremont-Bear Fire 2018, and (d) Camp Fire 2018.

In Figure 3, gray-filled areas represent the burned areas of the wildfires that occurred before and had already been contained on the ignition date shown in each panel. For instance, the gray-filled areas in Figure 3a showing the MDIGUST distribution on 16 August 2020 are the burned areas of the wildfires that occurred during 2017–2019 and of Gold Fire 2020, which was extinguished on 12 August 2020. Unfilled wildfire perimeters in Figure 3 are the burned areas of the wildfires that were still active (not fully contained) on the ignition date shown in each panel. Black square dots in each panel are the grid points whose daily averaged MDIGUST peaks on the shown date (i.e., ignition date for each fire) during the time period shown in Figure 2. Namely, the black square dots in each panel also include the ignition location grid of each selected wildfire, which is enclosed in a black circle. Moreover, black dotted lines in Figure 2 show the contours of daily averaged MDIGUST that were equal to or greater than the 80th percentile of daily averaged MDIGUST in North Coast and Sierra Nevada on the ignition date. These black square dots and black dotted lines allow us to identify areas where MDIGUST becomes high with respect to spatial distribution and where MDIGUST temporally peaks on the ignition date of each selected wildfire. We call the area where the black square dots are located and which is enclosed in a dotted line the "overlapping area" in the following.
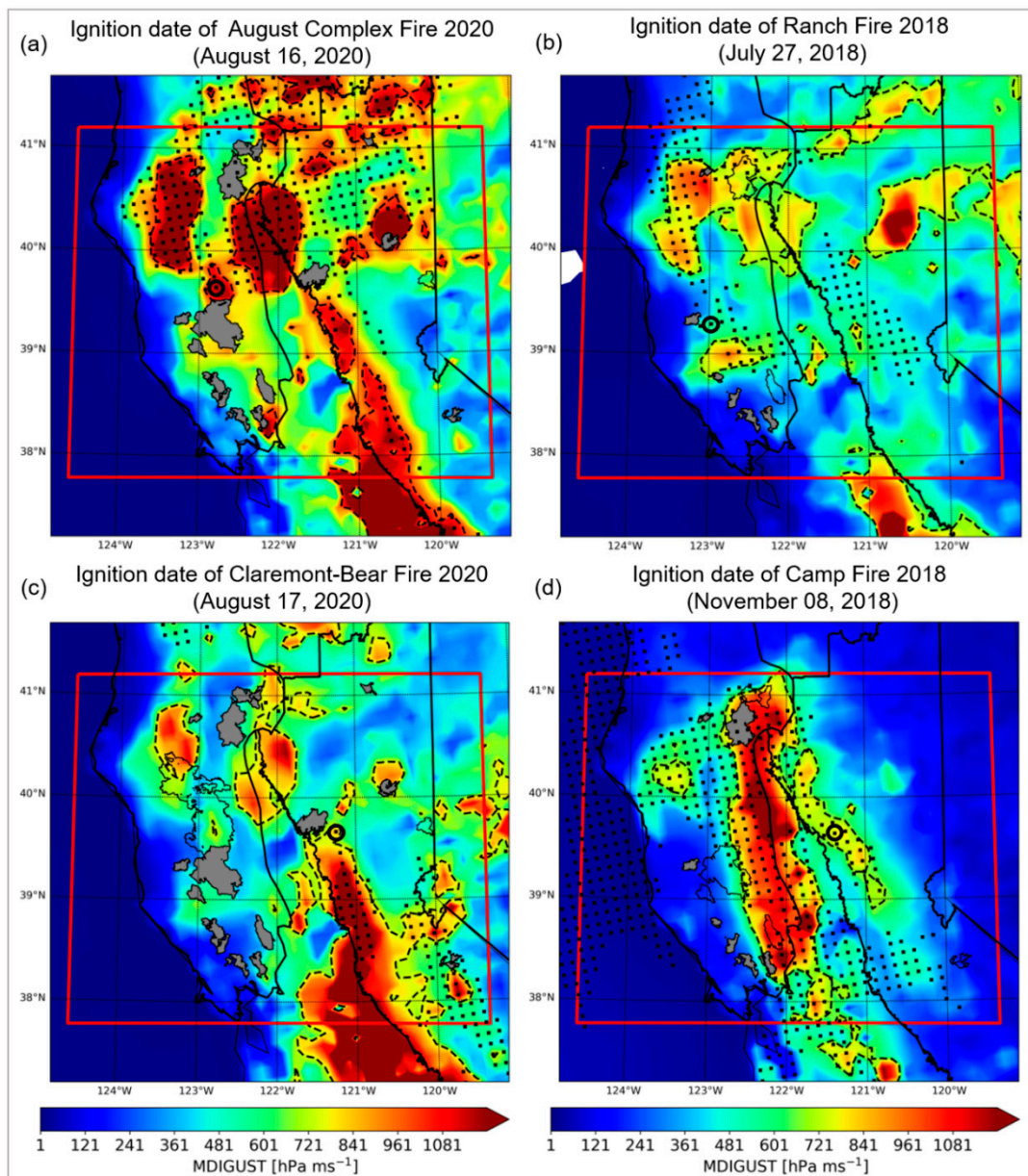
Figure 3. Spatial distributions of daily averaged MDIGUST on the ignition date for each wildfire. (**a**) August Complex Fire 2020, (**b**) Ranch Fire 2018, (**c**) Claremont-Bear Fire 2018, and (**d**) Camp Fire 2018. Gray-filled areas represent the burned areas of the wildfires that occurred before and had already been contained on the ignition date. Unfilled wildfire perimeters are the burned areas of the wildfires that were still active (not fully contained) on the ignition date. Black square dots are the grid points whose daily averaged MDIGUST peaked on the ignition date during the time period shown in Figure 2. Black dotted lines in Figure 2 show the contours of daily averaged MDIGUST that were equal to or greater than the 80th percentile of daily averaged MDIGUST in North Coast and Sierra Nevada on the ignition date. The ignition location grid point is enclosed in a black circle.

Figure 3a shows that the overlapping areas were mainly distributed in the middle to northern North Coast or the north-western Sierra Nevada on the ignition date of August Complex Fire 2020. An overlapping area can be found in the Northern Central Valley, which is lightly forested but not in the region of interest in this study. We can see that the ignition location of August Complex Fire 2020, enclosed in a circle, was located in the identified overlapping area in the middle of North Coast, although there were some other overlapping areas where MDIGUST became higher. In Figure 3c, on the ignition date of Claremont-Bear Fire 2020, the overlapping area was not really found over the North

Coast, despite the distribution of the large overlapping area on the day before (Figure 3a). It should be noted that the spatial distribution of MDIGUST changed drastically in one day. Figure 3c shows that the overlapping areas were mainly found in the south-western Sierra Nevada. Although the ignition location of Claremont-Bear Fire 2020 did not show a very large MDIGUST compared to the south-western Sierra Nevada, it was also located in the overlapping area. In Figure 3b, the overlapping areas can be found in the northern North Coast and southern North Coast on the ignition date of Ranch Fire 2018. Figure 3b shows that the ignition location of Ranch Fire 2018 was not located in the overlapping area since it showed moderate MDIGUST. Figure 3d shows that, on the ignition date of Camp Fire 2018, the overlapping areas were distributed mainly in the eastern North Coast and the western Sierra Nevada. The overlapping areas in Central Valley, again, were not the regions of interest in this study. Although the overlapping areas in the eastern North Coast showed much greater MDIGUST, the ignition location of Camp Fire 2018 was also located in the overlapping area in the western Sierra Nevada.

In summary, our analysis showed that August Complex Fire 2020, Claremont-Bear Fire 2020, and Camp Fire 2018 occurred in the identified overlapping areas. Ranch Fire 2018 occurred in the area that was not within the overlapping area but a short distance away from the overlapping area in the southern North Coast. On the basis of the above results, this analysis suggests that it may be possible to narrow down, to some extent, the potential locations with high risks of disastrous wildfire occurrences by using spatial and temporal hydrological/meteorological information, such as MDIGUST. As shown in Figure 3, these wildfires did not necessarily occur in the overlapping areas with the largest MDIGUST in the study area. It should be noted that the hydrological/meteorological conditions that are required for large fire occurrences and growths are location-dependent since the land cover, such as forest type, varies with location. Hence, the areas with the largest MDIGUST do not necessarily represent the largest wildfire risk areas.

3.4. Relationships between Burned Area Sizes and Hydrological/Meteorological Variables and Indices for the Target Wildfires

In this section, we further examined the correlation between hydrological/meteorological variables/indices and burned area sizes of the target wildfires at a longer time scale and larger spatial scale than the ignition date and ignition location scales. Figure 4 shows the correlation between the logarithms of burned area size and the hydrological/meteorological variables/indices for the target wildfires.

We used time-averaged daily spatial maximum (spatial minimum for soil moisture) variables/indices within the burned area during the 2 week period after the ignition date for each target wildfire. In Figure 4, although soil moisture content and burned area size showed a relatively weak correlation that was not statistically significant (R = -0.37, $p = 0.087$; Figure 4a), VPD correlated more strongly with the burned area (R = 0.60, $p = 0.003$; Figure 4b). Furthermore, horizontal wind speed showed stronger correlation with burned area size (R = 0.61, $p = 0.002$; Figure 4c) than wind gust speed (R = 0.43, $p = 0.049$; Figure 4d). Therefore, it can be inferred that horizontal wind speed controls the area sizes (i.e., growths) of the target wildfires more significantly than the wind gust speed does, while the wind gust speed explains the wildfire ignition better, as shown in Figures 2 and 3.

Compared to the above variables, the proposed indices overall showed higher correlations with burned area sizes. MDI, which evaluates the degree of comprehensive moisture deficit, correlates with burned area sizes slightly stronger than VPD (R = 0.62, $p = 0.002$; Figure 4e). The indices including moisture deficit and wind strength information, MDI-WIND and MDIGUST, showed an even higher correlation with burned area sizes. Among the hydrological/meteorological variables/indices considered, burned area sizes correlated most strongly with MDIWIND (R = 0.72, $p < 0.001$; Figure 4f), while MDIGUST showed a slightly weaker correlation with burned area sizes (R = 0.68, $p < 0.001$; Figure 4g). According to the above, the area sizes of the target wildfires are explained better by using the indices that evaluate the comprehensive moisture deficit and wind strength information.
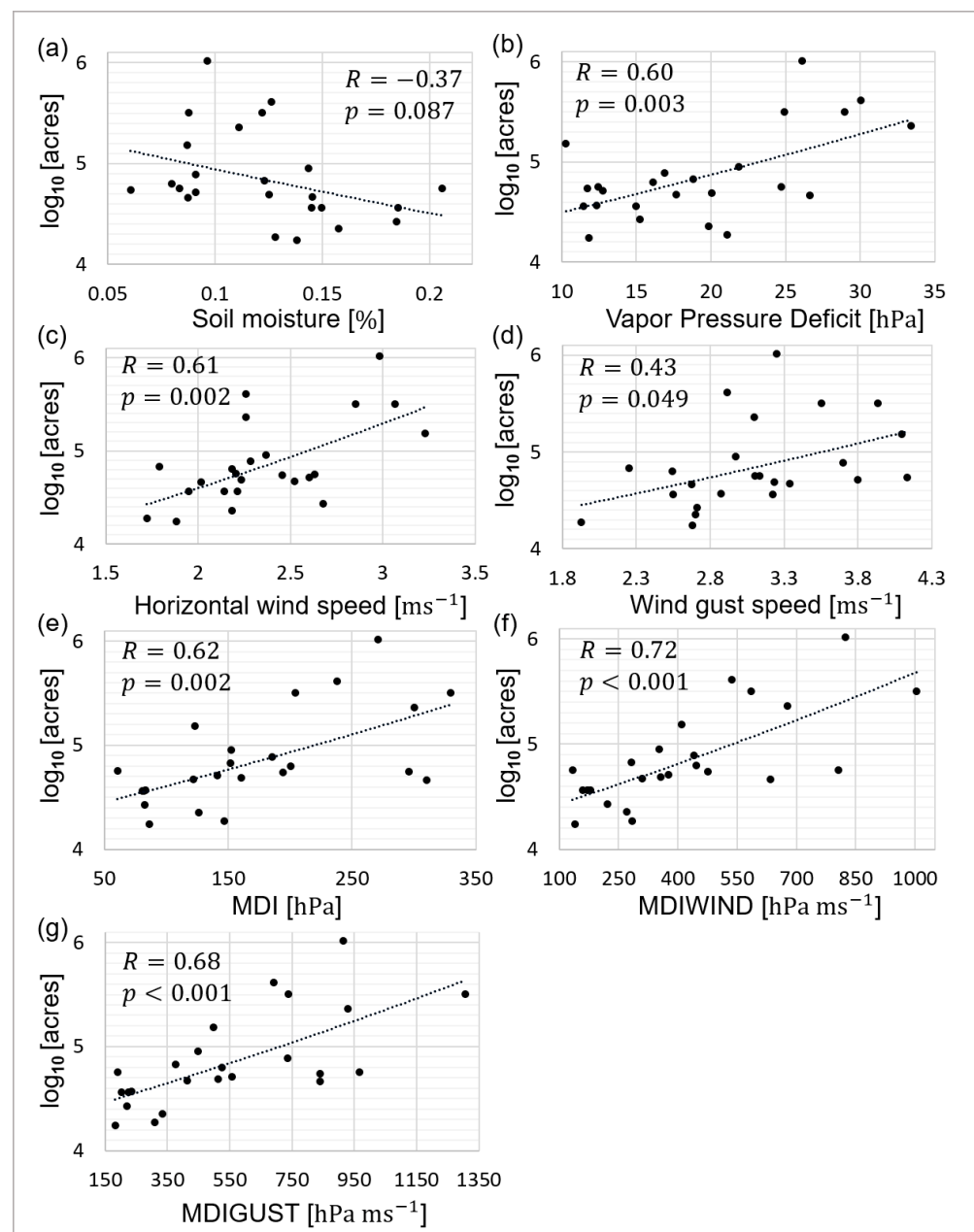
Figure 4. Correlation between the logarithms of burned area size and the hydrological/meteorological variables/indices for the target wildfires. (**a**) Soil moisture, (**b**) vapor pressure deficit, (**c**) horizontal wind speed, (**d**) wind gust speed, (**e**) Moisture Deficit Index (MDI), (**f**) MDIWIND, and (**g**) MDIGUST.

4. Discussion and Conclusions

This study was designed to evaluate the hydrological/meteorological controls on the recent large wildfires during 2017–2020 in Northern California at spatial and temporal scales of the wildfires' occurrence or growth. The main findings of this study are summarized below.

(1) Our analysis showed that the ignition location grids of the target wildfires generally have moisture deficit tendencies in fire-years compared to non-fire-years (Tables 2 and 3). Further, the ignition location MDIWIND and MDIGUST showed larger values in fire-years compared to non-fire-years for most of the target wildfires (95.8% and 91.7%, respectively). Other recent studies also reported that moisture deficits are strongly associated with wildfire regimes in the western United States [5,6].

(2) It was shown that the indices that comprehensively evaluate the effects of moisture deficit and wind strength explain the ignition timings better than MDI, which evaluates moisture deficit degree (Figure 2). Specifically, the MDIGUST peak's timing coincided with the ignition date for August Complex Fire 2020, Ranch Fire 2018, Claremont-Bear Fire 2020, and Camp Fire 2018. This finding suggests that when the risk of large wildfire occurrence becomes high at a certain location could be identified by using the comprehensive information of moisture deficit and of wind strength, which agrees with the finding of Srock et al. [22].

(3) The analysis of the spatial distribution of MDIGUST showed that August Complex Fire 2020, Claremont-Bear Fire 2020, and Camp Fire 2018 occurred in the identified overlapping areas where MDIGUST becomes spatially and temporally high (Figure 3). Although this analysis did not identify the exact ignition locations of the selected wildfires, it may be used to narrow down, to some extent, the potential locations with high risks of disastrous wildfire occurrences. In other words, this analysis is expected to provide useful information for identifying the regions to be monitored for high risk of catastrophic wildfire occurrences in the study area.

(4) We examined the correlation between the logarithms of burned area size and time-averaged daily spatial maximum/minimum variables and indices within the burned area during the 2 week period after the ignition date for target wildfires. We found strong relationships between burned area sizes of the target wildfires and VPD ($R = 0.60$, $p = 0.003$), MDI ($R = 0.62$, $p = 0.002$), MDIWIND ($R = 0.72$, $p < 0.001$; Figure 4f), and MDIGUST ($R = 0.68$, $p < 0.001$; Figure 4g). These results suggest that the combination of hot, dry, and windy weather and dry soil conditions strongly drive large wildfire activities in the study area. Similarly, Williams et al. [5] reported a strong correlation between burned area sizes and VPD ($R = 0.72$, $p = 0.003$) over the North Coast and the Sierra Nevada regions for summer wildfires during 1972–2018 in California.

The above findings could contribute to a more temporally and spatially detailed forecast of wildfire risks by using a regional climate model since these findings are obtained using the NCEP NAM 12 km Analysis that is produced by a regional climate model. Furthermore, these findings could lead to better management of future wildfire risks or a better understanding of wildfires' occurrence and growth mechanisms. There are some limitations, however, to this study. The limitations and future directions are summarized below.

First, although the analysis was conducted using NCEP NAM 12 km Analysis, it might be possible to clarify more robust hydrological/meteorological controls on the target wildfires by using finer resolution data. One may argue that the spatial resolution of 12 km is coarse for analyzing hydrological/meteorological conditions at the ignition locations. Thus, future work should include the downscaling of the historical atmospheric data for further analysis, as in the work of Abatzoglou and Brown [46] or in that of Carvalho et al. [47].

Second, the proposed indices, such as MDI, MDIWIND, and MDIGUST, were developed by simply multiplying or dividing the hydrological/meteorological variables. Although this simplicity can be interpreted as an advantage for practical use, there is a possibility that indices that more strongly account for wildfire regimes could be developed by using more complex functions. Future work should examine developing other indices that could explain wildfire regimes better.

Third, this study did not investigate the effect of fuel conditions on wildfire regimes. Besides hydrological/meteorological conditions, spatial and temporal information on fuel availability is considered to explain the wildfire regimes in more detail [48–50]. For instance, even under the ideal hydrological/meteorological condition for wildfires, the spread of wildfires can be limited by fuel availability [43]. Future work should examine large wildfire growths using spatial and temporal fuel information, such as fuel availability, fuel types, and fuel moisture [51].

Lastly, we compared the hydrological/meteorological conditions in fire-years and non-fire-years by focusing on the time period of 2012–2020 due to the data availability. Yet, consideration of a longer period could lead to a more evident differences in hydrological/meteorological conditions between fire-years and non-fire years. Hence, a longer study period should be considered in future work. However, even when focusing on only relatively recent years (i.e., usually too short a period to discuss the climate change effects), fire-years still showed distinctive hydrological/meteorological conditions compared to non-fire-years, as shown in Tables 2 and 3. Therefore, investigating causes of those unusual hydrological/meteorological conditions, such as moisture deficit conditions, is another important subject for future studies.

It should also be noted that, in order to achieve a better forecast of wildfire risks or strategic fire management, considering not only hydrological/meteorological factors but also human factors is of significant importance. In fact, Faivre et al. [52] showed that the distance to a road and distance to housing were important determinants of ignition frequency in Southern California. Yang et al. [53] found that human accessibility and land ownership were primary factors in shaping clustered fire origin locations. Therefore, in future work, it would be of great interest to incorporate the effect of human factors into the hydrological/meteorological controls found in this study.

Author Contributions: Conceptualization, Y.H. and M.L.K.; methodology, Y.H.; investigation, Y.H.; writing—original draft preparation, Y.H.; writing—review and editing, M.L.K.; visualization, Y.H.; supervision, M.L.K. All authors have read and agreed to the published version of the manuscript.

References

1. CALFIRE Incidents. California Department of Forestry and Fire Protection (CAL FIRE). Incident Archive. 2020. Available online: https://www.fire.ca.gov/incidents/ (accessed on 10 April 2021).
2. Wang, D.; Guan, D.; Zhu, S.; Kinnon, M.M.; Geng, G.; Zhang, Q.; Zheng, H.; Lei, T.; Shao, S.; Gong, P.; et al. Economic footprint of California wildfires in 2018. *Nat. Sustain.* **2018**, *4*, 252–260. [CrossRef]
3. Proctor, C.R.; Lee, J.; Yu, D.; Shah, A.D.; Whelton, A.J. Wildfire caused widespread drinking water distribution network contamination. *AWWA Water Sci.* **2020**, *2*, 1–14. [CrossRef]
4. Williams, A.P.; Abatzoglou, J.T.; Gershunov, A. Observed Impacts of Anthropogenic Climate Change on Wildfire in California. *Earth Future* **2019**, *7*, 892–910. [CrossRef]
5. Abatzoglou, J.T.; Williams, A.P. Impact of anthropogenic climate change on wildfire across western US forests. *Proc. Natl. Acad. Sci. USA* **2016**, *113*, 11770–11775. [CrossRef] [PubMed]
6. Holden, Z.A.; Swanson, A.; Luce, C.H.; Jolly, W.M.; Maneta, M.; Oyler, J.W.; Warren, D.A.; Parsons, R.; Affleck, D. Decreasing fire season precipitation increased recent western US forest wildfire activity. *Proc. Natl. Acad. Sci. USA* **2018**, *115*, E8349–E8357. [CrossRef]
7. Westerling, A.L.R. Increasing western US forest wildfire activity: Sensitivity to changes in the timing of spring. *Philos. Trans. R. Soc. B Biol. Sci.* **2016**, *371*, 20150178. [CrossRef]
8. Westerling, A.L.; Hidalgo, H.G.; Cayan, D.R.; Swetnam, T.W. Warming and earlier spring increase Western U.S. forest wildfire activity. *Science* **2006**, *313*, 940–943. [CrossRef] [PubMed]
9. Mass, C.F.; Ovens, D. The northern California wildfires of 8–9 October 2017. *Bull. Am. Meteorol. Soc.* **2019**, *100*, 235–256. [CrossRef]

10. Nauslar, N.J.; Abatzoglou, J.T.; Marsh, P.T. The 2017 North Bay and Southern California Fires: A Case Study. *Fire* **2018**, *1*, 18. [CrossRef]
11. Fovell, R.G.; Gallagher, A. Winds and Gusts during the Thomas Fire. *Fire* **2018**, *1*, 47. [CrossRef]
12. Rolinski, T.; Capps, S.B.; Fovell, R.G.; Cao, Y.; D'Agostino, B.J.; Vanderburg, S. The Santa Ana wildfire threat index: Methodology and operational implementation. *Weather Forecast* **2016**, *31*, 1881–1897. [CrossRef]
13. Smith, C.; Hatchett, B.J.; Kaplan, M. A Surface Observation Based Climatology of Diablo-Like Winds in California's Wine Country and Western Sierra Nevada. *Fire* **2018**, *1*, 25. [CrossRef]
14. Gedalof, Z.E.; Peterson, D.L.; Mantua, N.J. Atmospheric, climatic, and ecological controls on extreme wildfire years in the northwestern United States. *Ecol. Appl.* **2005**, *15*, 154–174. [CrossRef]
15. Parisien, M.A.; Moritz, M.A. Environmental controls on the distribution of wildfire at multiple spatial scales. *Ecol. Monogr.* **2009**, *79*, 127–154. [CrossRef]
16. Nunes, L.J.; Raposo, M.A.; Pinto Gomes, C.J. A Historical Perspective of Landscape and Human Population Dynamics in Guimarães (Northern Portugal): Possible Implications of Rural Fire Risk in a Changing Environment. *Fire* **2021**, *4*, 49. [CrossRef]
17. Goss, M.; Swain, D.L.; Abatzoglou, J.T.; Sarhadi, A.; Kolden, C.A.; Williams, A.P.; Diffenbaugh, N.S. Climate change is increasing the likelihood of extreme autumn wildfire conditions across California. *Environ. Res. Lett.* **2020**, *15*, 094016. [CrossRef]
18. Westerling, A.L.; Bryant, B.P.; Preisler, H.K.; Holmes, T.P.; Hidalgo, H.G.; Das, T.; Shrestha, S.R. Climate change and growth scenarios for California wildfire. *Clim. Change* **2011**, *109*, 445–463. [CrossRef]
19. Di Giuseppe, F.; Vitolo, C.; Krzeminski, B.; San-Miguel, J. Fire weather index: The skill provided by ECMWF ensemble prediction system. *Nat. Hazards Earth Syst. Sci.* **2020**, *2020*, 1–18. [CrossRef]
20. Van Wagner, C.E. The development and structure of the Canadian Forest Fire Weather Index System. In *Forestry Technical Report*; Canadian Forest Service: Ottawa, ON, Canada, 1987; Volume 35, p. 37.
21. Westerling, A.L.; Cayan, D.R.; Brown, T.J.; Hall, B.L.; Riddle, L.G. Climate, santa ana winds and autumn wildfires in Southern California. *Eos* **2004**, *85*, 289–296. [CrossRef]
22. Srock, A.F.; Charney, J.J.; Potter, B.E.; Goodrick, S.L. The Hot-Dry-Windy Index: A New Fire Weather Index. *Atmosphere* **2018**, *9*, 279. [CrossRef]
23. McDonald, J.M.; Srock, A.F.; Charney, J.J. Development and application of a Hot-Dry-Windy Index (HDW) climatology. *Atmosphere* **2018**, *9*, 285. [CrossRef]
24. Potter, B.; Charney, J.; Srock, A. The Hot-Dry-Windy Index: A New Tool for Forecasting Fire Weather. In *Science Findings 227*; US Department of Agriculture, Forest Service, Pacific Northwest Research Station: Portland, OR, USA, 2020; pp. 1–5.
25. Hyoung, L.J. Prediction of Large-Scale Wildfires with the Canopy Stress Index Derived from Soil Moisture Active Passive. *IEEE J. Sel. Top. Appl. Earth Obs. Remote Sens.* **2021**, *14*, 2096–2102. [CrossRef]
26. Krueger, E.S.; Ochsner, T.E.; Carlson, J.D.; Engle, D.M.; Twidwell, D.; Fuhlendorf, S.D. Concurrent and antecedent soil moisture relate positively or negatively to probability of large wildfires depending on season. *Int. J. Wildl. Fire.* **2016**, *25*, 657–668. [CrossRef]
27. Krueger, E.S.; Ochsner, T.E.; Quiring, S.M.; Engle, D.M.; Carlson, J.D.; Twidwell, D.; Fuhlendorf, S.D. Measured Soil Moisture is a Better Predictor of Large Growing-Season Wildfires than the Keetch-Byram Drought Index. *Soil Sci. Soc. Am. J.* **2017**, *81*, 490–502. [CrossRef]
28. Ambadan, J.T.; Oja, M.; Gedalof, Z.; Berg, A.A. Satellite-Observed Soil Moisture as an Indicator of Wildfire Risk. *Remote Sens.* **2020**, *12*, 1543. [CrossRef]
29. Jensen, D.; Reager, J.T.; Zajic, B.; Rousseau, N.; Rodell, M.; Hinkley, E. The sensitivity of US wildfire occurrence to pre-season soil moisture conditions across ecosystems. *Environ. Res. Lett.* **2018**, *13*, 014021. [CrossRef]
30. Schaefer, A.J.; Magi, B.I. Land-cover dependent relationships between fire and soil moisture. *Fire* **2019**, *2*, 55. [CrossRef]
31. Rigden, A.J.; Powell, R.S.; Trevino, A.; McColl, K.A.; Huybers, P. Microwave Retrievals of Soil Moisture Improve Grassland Wildfire Predictions. *Geophys. Res. Lett.* **2020**, *47*, 1–8. [CrossRef]
32. Sungmin, O.; Hou, X.; Orth, R. Observational evidence of wildfire-promoting soil moisture anomalies. *Sci. Rep.* **2020**, *10*, 1–8. [CrossRef]
33. Waring, R.H.; Coops, N.C. Predicting large wildfires across western North America by modeling seasonal variation in soil water balance. *Clim. Chang.* **2016**, *135*, 325–339. [CrossRef]
34. Kumar, V.; Dharssi, I. Evaluation and calibration of a high-resolution soil moisture product for wildfire prediction and management. *Agric. For. Meteorol.* **2019**, *264*, 27–39. [CrossRef]
35. Balch, J.K.; Bradley, B.A.; Abatzoglou, J.T.; Chelsea Nagy, R.; Fusco, E.J.; Mahood, A.L. Human-started wildfires expand the fire niche across the United States. *Proc. Natl. Acad. Sci. USA* **2017**, *114*, 2946–2951. [CrossRef]
36. InciWeb. Incident Information System. 2020. Available online: https://inciweb.nwcg.gov/incident/ (accessed on 10 April 2021).
37. Eidenshink, J.; Schwind, B.; Brewer, K.; Zhu, Z.-L.; Quayle, B.; Howard, S. A Project for Monitoring Trends in Burn Severity. *Fire Ecol.* **2007**, *3*, 3–21. [CrossRef]
38. California State Geoportal Wildfire Perimeters. California Department of Technology. 2020. Available online: https://gis.data.ca.gov/datasets/f72ebe741e3b4f0db376b4e765728339_0?geometry=-133.004%2C35.454%2C-110.547%2C41.470 (accessed on 10 April 2021).

39. National Centers for Environmental Prediction (NCEP), National Weather Service (NWS)/NOAA/U.S. Department of Commerce (DOC). National Center for Atmospheric Research, Computational and Information Systems Laboratory, NCEP North American Mesoscale (NAM) 12 km Analysis. 2021. Available online: https://rda.ucar.edu/datasets/ds609.0/ (accessed on 10 April 2021).
40. Bolton, D. The computation of equivalent potential temperature. *Mon. Weather Rev.* **1980**, *111*, 1859–1871. [CrossRef]
41. Gutiérrez, A.; Fovell, R.G. A new gust parameterization for weather prediction models. *J. Wind Eng. Ind. Aerodyn.* **2018**, *177*, 45–59. [CrossRef]
42. Running, S.W. Is global warming causing more, larger wildfires? *Science* **2006**, *313*, 927–928. [CrossRef] [PubMed]
43. Westerling, A.L.; Bryant, B.P. Climate change and wildfire in California. *Clim. Chang.* **2008**, *87*, 231–249. [CrossRef]
44. National Integrated Drought Information System (NIDIS). What Is Soil Moisture? 2021. Available online: https://www.drought.gov/topics/soil-moisture (accessed on 10 April 2021).
45. National Weather Service (NWS). Changes to the Surface Wind Gust Speed Calculation in the NAM and DGEX. National Technical Imprementation Notice. 2012. Available online: http://www.nws.noaa.gov/os/notif.htm (accessed on 10 April 2021).
46. Abatzoglou, J.T.; Brown, T.J. A comparison of statistical downscaling methods suited for wildfire applications. *Int. J. Climatol.* **2012**, *32*, 772–780. [CrossRef]
47. Carvalho, A.C.; Carvalho, A.; Martins, H.; Marques, C.; Rocha, A.; Borrego, C.; Viegas, D.X.; Miranda, A.I. Fire weather risk assessment under climate change using a dynamical downscaling approach. *Environ. Model. Softw.* **2011**, *26*, 1123–1133. [CrossRef]
48. Keeley, J.E.; Syphard, A.D. Twenty-first century California, USA, wildfires: Fuel-dominated vs. wind-dominated fires. *Fire Ecol.* **2019**, *15*, 24. [CrossRef]
49. Littell, J.S.; Peterson, D.L.; Riley, K.L.; Liu, Y.; Luce, C.H. A review of the relationships between drought and forest fire in the United States. *Glob. Chang. Biol.* **2016**, *22*, 2353–2369. [CrossRef] [PubMed]
50. Walker, X.J.; Rogers, B.M.; Veraverbeke, S.; Johnstone, J.F.; Baltzer, J.L.; Barrett, K.; Bourgeau-Chavez, L.; Day, N.J.; de Groot, W.J.; Dieleman, C.M.; et al. Fuel availability not fire weather controls boreal wildfire severity and carbon emissions. *Nat. Clim. Chang.* **2020**, *10*, 1130–1136. [CrossRef]
51. Littell, J.S.; Mckenzie, D.; Peterson, D.L.; Westerling, A.L. Climate and wildfire area burned in western U.S. ecoprovinces, 1916–2003. *Ecol. Appl.* **2009**, *19*, 1003–1021. [CrossRef] [PubMed]
52. Faivre, N.; Jin, Y.; Goulden, M.L.; Randerson, J.T. Controls on the spatial pattern of wildfire ignitions in Southern California. *Int. J. Wildl. Fire* **2014**, *23*, 799–811. [CrossRef]
53. Yang, J.; He, H.S.; Shifley, S.R. Spatial controls of occurrence and spread of wildfires in the Missouri Ozark Highlands. *Ecol. Appl.* **2008**, *18*, 1212–1225. [CrossRef]